Formation of Glaciers on Mars by Atmospheric Precipitation at High Obliquity

F. Forget, *et al.*

Science **311**, 368 (2006);
DOI: 10.1126/science.1120335

Science (print ISSN 0036-8075; online ISSN 1095-9203) is published weekly, except the last week in December, by the American Association for the Advancement of Science, 1200 New York Avenue NW, Washington, DC 20005.

that firm conclusions about the effects of the p-H_2 matrix on the methanol torsion-vibration spectral structure would be premature at this stage without more definitive gas-phase data.

Taken together, these results suggest that the p-H_2 matrix will serve as an important medium for the study of large-amplitude vibrational motions and molecular spin conversion processes, providing valuable information to aid our understanding of complicated spectral patterns both in the gas phase and in molecular ices.

References and Notes

1. T. Oka, *Annu. Rev. Phys. Chem.* **44**, 299 (1993).
2. T. Momose, T. Shida, *Bull. Chem. Soc. Jpn.* **71**, 1 (1998).
3. K. Yoshioka, D. T. Anderson, *J. Chem. Phys.* **119**, 4731 (2003).
4. S. Tam *et al.*, *J. Chem. Phys.* **111**, 4191 (1999).
5. T. Momose *et al.*, *J. Chem. Phys.* **103**, 1400 (1995).
6. T. Momose *et al.*, *J. Chem. Phys.* **107**, 7707 (1997).
7. R. L. Redington, D. E. Milligan, *J. Chem. Phys.* **39**, 1276 (1963).
8. F. H. Frayer, G. E. Ewing, *J. Chem. Phys.* **48**, 781 (1968).
9. H. P. Hopkins, R. F. Curl, K. S. Pitzer, *J. Chem. Phys.* **48**, 2959 (1968).
10. We have developed a pulsed-deposition technique that can operate at a deposition temperature up to 5.5 K (*21*). Thus, it is suitable for use with our previous cryogenic refrigerator that cools to only ~5 K. As well, with a new closed-cycle refrigerator system (Janis RDK-415) capable of cooling the sample target to 3.5 K, we could use conventional continuous deposition with a flow rate of ~0.03 mol hour^{-1}.
11. CH_3OH (99.9%, Mallinckrodt, analytical reagent grade) was purified by passing the vapor though P_2O_5 to remove trace water impurity. H_2 (99.9999%, Scott Specialty Gases) was used after passage through a trap at 77 K before conversion to p-H_2. The p-H_2 converter comprised a copper cell filled with $Fe(OH)_3$ catalyst and cooled with a closed-cycle refrigerator. The efficiency of conversion is controlled by the temperature of the catalyst; at 15 K, the concentration of o-H_2 is ~100 ppm.
12. Any mention of commercial products in this paper is for information only; it does not imply recommendation or endorsement by NIST.
13. L.-H. Xu *et al.*, *J. Mol. Spectrosc.* **228**, 453 (2004).
14. G. Moruzzi, B. P. Winnewisser, M. Winnewisser, I. Mukhopadhyay, F. Strumia, *Microwave, Infrared and Laser Transitions of Methanol: Atlas of Assigned Lines from 0 to 1258 cm^{-1}* (CRC Press, Boca Raton, FL, 1995).
15. L.-H. Xu *et al.*, *J. Mol. Spectrosc.* **185**, 158 (1997).
16. X. Wang, D. S. Perry, *J. Chem. Phys.* **109**, 10795 (1998).
17. I. Kleiner, G. T. Fraser, J. T. Hougen, A. S. Pine, *J. Mol. Spectrosc.* **147**, 155 (1991).
18. M. A. Temsamani, L.-H. Xu, R. M. Lees, *J. Mol. Spectrosc.* **218**, 220 (2003).
19. R. M. Lees *et al.*, *J. Mol. Spectrosc.* **228**, 528 (2004).
20. R. M. Lees, L.-H. Xu, *Phys. Rev. Lett.* **84**, 3815 (2000).
21. Y.-J. Wu, X. Yang, Y.-P. Lee, *J. Chem. Phys.* **120**, 1168 (2004).
22. X. Wang, D. S. Perry, L.-H. Xu, unpublished data.
23. B. N. Taylor, C. E. Kugatt, *NIST Tech. Note 1297* (1994).

24. Supported by the Natural Sciences and Engineering Research Council of Canada (R.M.L. and L.H.X.) and by National Science Council of Taiwan grant NSC94-2113-M-009-017.

12 October 2005; accepted 12 December 2005
10.1126/science.1121300

Formation of Glaciers on Mars by Atmospheric Precipitation at High Obliquity

F. Forget,[1]* R. M. Haberle,[2] F. Montmessin,[3] B. Levrard,[4] J. W. Head[5]

Surface conditions on Mars are currently cold and dry, with water ice unstable on the surface except near the poles. However, geologically recent glacierlike landforms have been identified in the tropics and the midlatitudes of Mars. The ice has been proposed to originate from either a subsurface reservoir or the atmosphere. We present high-resolution climate simulations performed with a model designed to simulate the present-day Mars water cycle but assuming a 45° obliquity as experienced by Mars a few million years ago. The model predicts ice accumulation in regions where glacier landforms are observed, on the western flanks of the great volcanoes and in the eastern Hellas region. This agreement points to an atmospheric origin for the ice and reveals how precipitation could have formed glaciers on Mars.

Among the most striking recent observations by the cameras aboard the Mars Express, Mars Global Surveyor (MGS), and Mars Odyssey orbiters are low-latitude, geologically recent, morphological features that clearly formed by the action of a water ice glacier (*1*–*8*). The most characteristic landforms appear to be clustered in several specific regions that had already been identified in Viking images (*9*, *10*). First, each of the Tharsis Montes volcanoes has a fan-shaped deposit near its northwestern flank (Fig. 1A), interpreted to be the remains of geologically recent glaciers (*3*, *4*). In the same region, debris-covered piedmont glaciers along the northwest edge of the Olympus Mons scarp (Fig. 1A) were seen in Viking and Mars Odyssey Thermal Emission Imaging System (THEMIS) data (*8*, *10*). Recent images of these glacier remnants obtained by the Mars Express High Resolution Stereo Camera (HRSC) show that they are covered by very recent rock glaciers (*1*, *2*). A second notable region is a relatively small area (1000 km across) on the eastern side of the Hellas Basin (90° to 120°E and 32° to 50°S), where some of the most spectacular examples of ice-related landforms are seen. More than 90 large lobate debris aprons up to 50 km across have been identified there (*5*, *9*). Some of these debris aprons are interpreted to represent very ice-rich debris-covered glaciers (*1*). Eastern Hellas also contains a variety of smaller ice-rich flow features, including tongue-shaped lobes observed at 247°W 38.6°S (*6*), hourglass-shaped craters apparently filled by a flowing debris-covered glacier (*1*), and many of the ice-cemented mantling deposits associated with gullies (*11*). A third major area of icy Mars is the Deuteronilus–Protonilus Mensae region (0° to 80°E and 30° to 50°N) (*9*), where large concentrations of lobate debris aprons and lineated valley fills (that resemble flow lines in glacial ice on Earth) are found. Outside these three regions, glacier-like features have been observed at mid-latitudes (*7*, *9*) but in more localized or limited forms.

Where did the ice come from? It has been suggested that the features could have been emplaced by creep or a landslide of material rich in ground ice (*12*, *13*) or released from a subsurface ground ice or groundwater reservoir (*2*). A recent analysis of the HRSC images of the western edge of Olympus Mons (*2*) concluded that the observations yielded evidence for hydrothermal mobilization of water with subsequent development of glaciers. However, the geomorphologic characteristic of most glacier features is also consistent with an atmospheric precipitation origin (*1*, *3*, *4*, *7*, *8*). This hypothesis has been supported by climate model simulations that suggested that, during a period of obliquity greater than about 35° to 45° (obliquity is the tilt of the planet's spin axis), the north polar water ice may be mobilized southward and deposited at lower latitudes (*14*–*16*). However, the simple cloud ice microphysics and the coarse spatial resolutions used by these previous models did not allow a true comparison between the modeled ice accumulations and the available geological observations.

[1]Laboratoire de Météorologie Dynamique, Institut Pierre Simon Laplace, Université Paris 6 Boite Postale 99, 75252 Paris cedex 05, France. [2]Space Science Division, Mail Stop 245-3, NASA Ames Research Center, Moffett Field, CA 94035, USA. [3]Service D'Aéronomie, Institut Pierre Simon Laplace, Université Paris 6 Box Postale 102, 75252 Paris cedex 05, France. [4]Astronomie et Systèmes Dynamiques, Institut de Mécanique Céleste, 77 Avenue Denfert Rochereau, 75014 Paris, France. [5]Department of Geological Sciences, Brown University, Providence, RI 02912, USA.

*To whom correspondence should be addressed. E-mail: forget@lmd.jussieu.fr

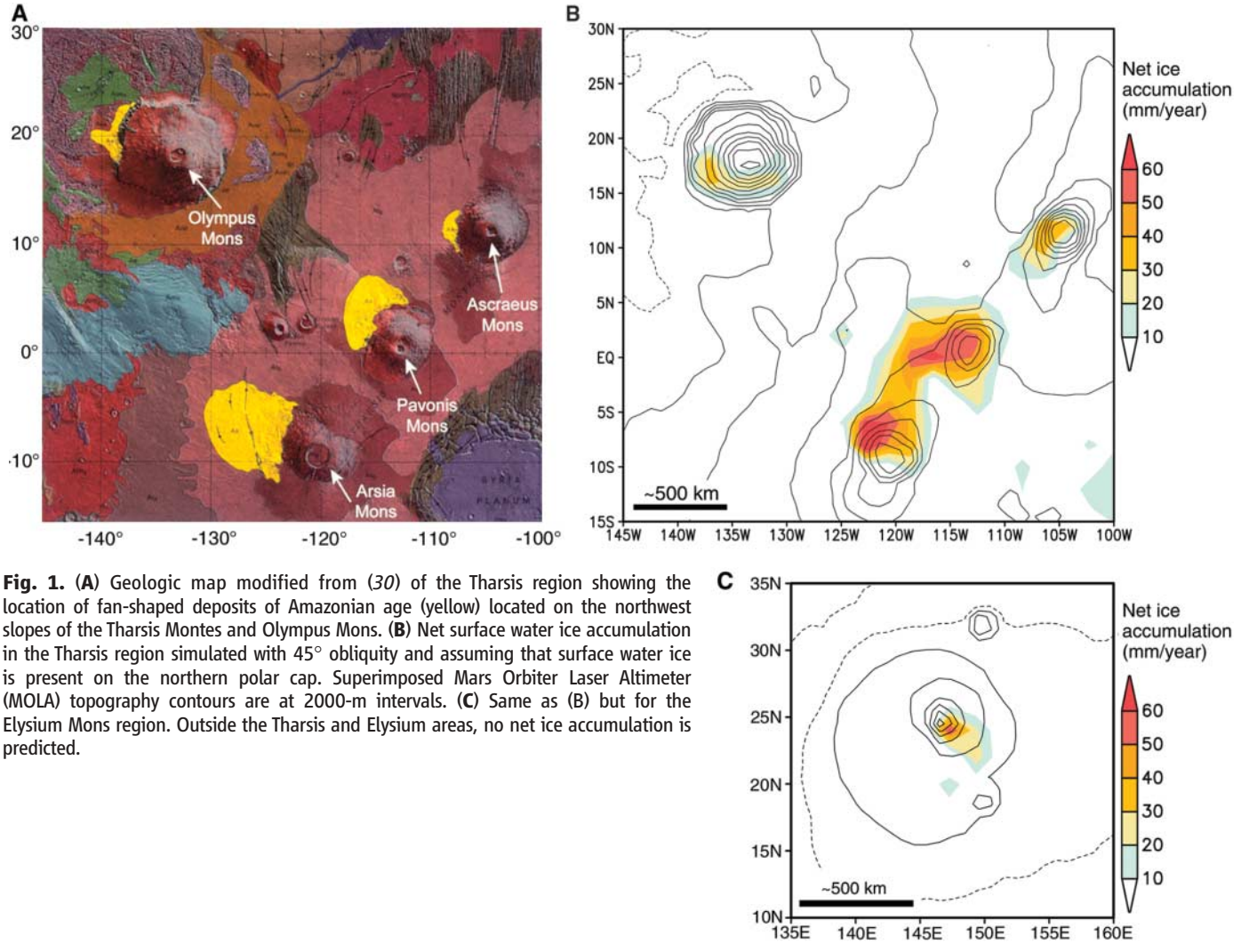

Fig. 1. (**A**) Geologic map modified from (*30*) of the Tharsis region showing the location of fan-shaped deposits of Amazonian age (yellow) located on the northwest slopes of the Tharsis Montes and Olympus Mons. (**B**) Net surface water ice accumulation in the Tharsis region simulated with 45° obliquity and assuming that surface water ice is present on the northern polar cap. Superimposed Mars Orbiter Laser Altimeter (MOLA) topography contours are at 2000-m intervals. (**C**) Same as (B) but for the Elysium Mons region. Outside the Tharsis and Elysium areas, no net ice accumulation is predicted.

Here, we use the martian global climate model of the Laboratoire de Météorologie Dynamique (LMD), which is designed to simulate the present-day climate on Mars (*17*). In particular, it provides distributions of atmospheric vapor and clouds in very good agreement with MGS Thermal Emission Spectrometer (TES) observations (*18*). It includes a full description of exchange between surface ice, atmospheric water, and transport and turbulent mixing of water in the atmosphere and a parameterization of the microphysics of cloud formation. The radiative effects of water vapor and clouds as well as the exchange of water vapor with the subsurface are not included.

To simulate a typical high-obliquity climate, we performed a simulation similar to the one presented in (*18*) for present-day Mars, except for the following modifications. First, in order not to favor any hemisphere, we set the orbit eccentricity to zero and fixed the reference visible dust optical depth (*19*) to a constant value (0.2). Second, we increased the obliquity of the planet to 45°. Such an obliquity has probably been common throughout Mars history (*20*). It last occurred on Mars 5.51×10^6 years ago and is close to the most probable value throughout Mars' history (41.8°) (*20*). Last, to better represent the atmosphere-topography interaction, we used a higher spatial resolution of 2° in latitude and 2.045° longitude (*21*).

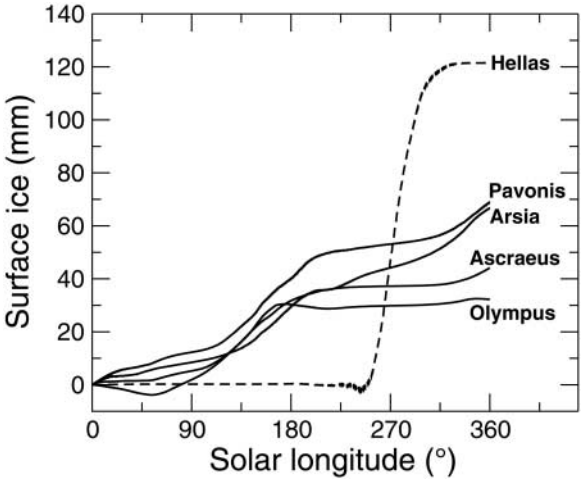

Fig. 2. Seasonal evolution of the ice accumulation over one martian year at several locations for our 45° obliquity simulations with a water ice northern polar cap (solid lines) and one simulation with a water ice southern polar cap (dashed line) near Pavonis Mons (117°W 0°N), near Arsia Mons (122°W 6°S), near Ascraeus Mons (107° W 12°N), near Olympus Mons (137°W, 16°N), and in Eastern Hellas (110°E, 40°S). Solar longitude (Ls) is the areocentric longitude of the sun, with Ls equal to 0° at northern spring equinox, 90° at summer solstice, 180° at autumn equinox, and 270° at winter solstice.

As predicted by previous climate simulations (*22*), the increased polar summer insolation enhances the polar ice sublimation and leads to a water cycle that is much more

intense than today's, with a column water abundance up to 3000 precipitable micrometers (pr-μm) above the northern polar cap around summer solstice and about 50 pr-μm in the summer tropics. Water ice accumulation reaching 30 to 70 mm per year occurs in five localized areas on the flanks of the Tharsis, Olympus, and Elysium Montes (Fig. 1, B and C), and nowhere else. After a few thousand years, such accumulations would form glaciers several hundred meters thick, and their locations can be compared to the locations of the glacier-related deposits observed in the Tharsis region (Fig. 1A). The agreement is excellent, with maximum deposition predicted on the western flanks of Arsia and Pavonis where the largest deposits are observed (Fig. 1A) (*3*, *4*) and lower deposition on the flanks of Ascraeus and Olympus. Precipitation is predicted in the upper part of the large area actually covered by the extensive Arsia Mons fan-shaped deposits, which appears to coincide with the accumulation zone of the more extensive glacial deposit (*3*).

Why does ice accumulate on the flanks of these mountains? In our simulation, most of the ice condenses in the lower atmosphere below 2 km. Precipitation occurs on Arsia and Pavonis all year long, whereas Olympus and Ascraeus only get ice during the northern summer (Fig. 2). During that season, large amounts of ice tend to condense out on the western side of the volcanoes because of strong westerly winds blowing upslope. In such a flow, the water-rich air is adiabatically cooled by 10 to 20 K (Fig. 3). Water condenses and forms ice particles of 20 to 50 μm in diameter that sediment onto the surface [compared to 6 to 8 μm in the present-day Tharsis clouds (*23*)]. The weather pattern that creates the strong westerly wind on Olympus in summer is comparable to the summer monsoon in Asia (fig. S1). At other seasons, Olympus and Ascraeus Montes do not receive precipitation because they are exposed to weaker winds and a drier atmosphere, whereas Arsia and Pavonis Montes continue to accumulate ice because of a symmetrical southern hemisphere monsoon circulation during southern spring and summer. Although our simulation predicts the accumulation of ice only on the flanks of the largest mountains, it is likely that this process occurred at smaller scales not resolved by our model, like on the subgrid-size Hecates Tholus near Elysium, where recent glacial deposits have been observed (*7*).

The location of the ice deposits predicted by our model and the accumulation rates are not too sensitive to the orbital parameters as long as the obliquity is above 40°. If the water input is enhanced by further raising the obliquity, by increasing the eccentricity with a perihelion in northern summer, or by assuming a larger northern ice cap, the model predicts an extension of the area where water ice can accumulate in the Tharsis Montes region toward Alba Patera.

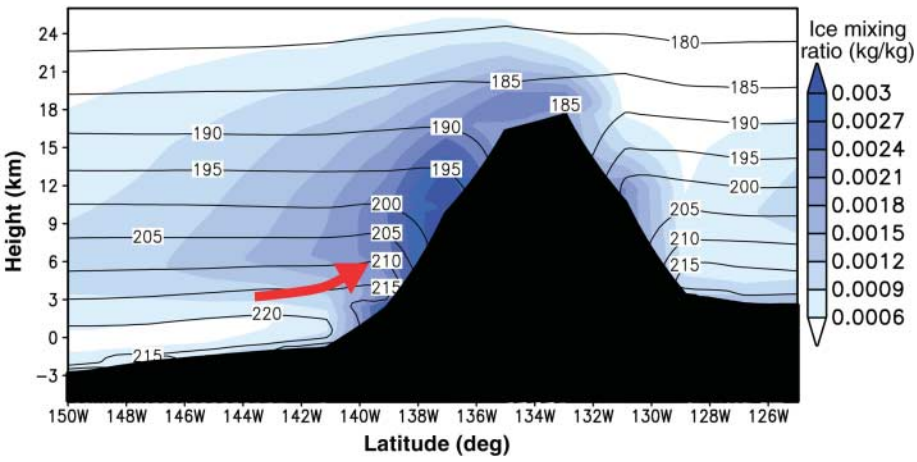

Fig. 3. Cross section of Olympus Mons along the 16°N latitude showing the mean atmospheric ice mass mixing ratio (shaded blue) and the atmospheric temperature (contour, K) averaged over the period of ice accumulation Ls = 125° to 155° (northern summer). The strong northwesterly winds induce adiabatic cooling on the flank of the volcanoes and atmospheric condensation and precipitation.

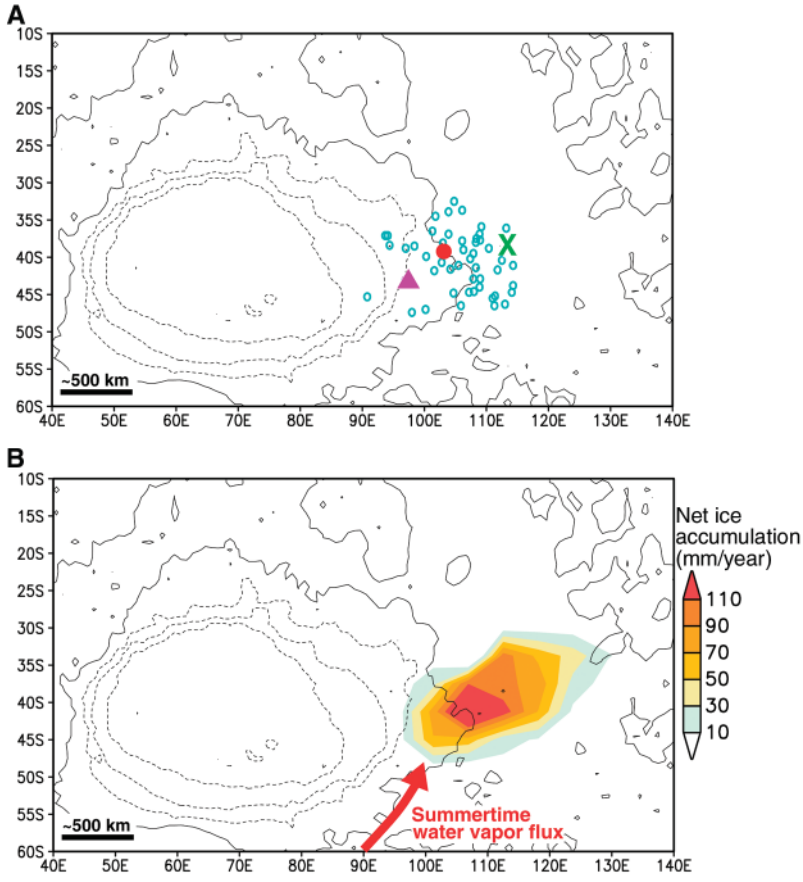

Fig. 4. (**A**) Topographic map of the Hellas Basin with contours every 2 km showing the locations of 54 debris apron complexes (*5*) (blue circles), which are interpreted as ice-rich flow features, the glacier-like landforms recently observed by Mars Express (*1*) (purple triangle, debris apron; red dot, hourglass-shaped deposits), and one of the most spectacular tongue-shaped rock glacier (green cross) observed on Mars (*6*). (**B**) Net surface water ice accumulation (in mm per martian year) predicted in the same area by our simulation performed with 45° obliquity and assuming that surface water ice is initially present only in the southern polar cap.

The north polar cap may not have always been the only source of water during high-obliquity periods. The presence of southern

polar deposits (*24*) and climate model simulations with orbital parameters different than today (*25*) suggest that the south polar region could also have played this role. On this basis, we performed a high-obliquity simulation assuming that ice was available in the south polar region (between 90°S and 80°S) rather than in the north. Under such conditions, ice accumulation still occurs in the southern part of Tharsis (Arsia-Pavonis Montes region and in Syria Planum), but the highest rates are then predicted to be in the eastern Hellas region (Fig. 4), almost exactly where the concentration of ice-related landforms is observed. Interestingly, the process leading to ice precipitation differs from the one occurring on the volcanoes. In eastern Hellas, almost all the ice is accumulated during a 90-day period around southern summer solstice (Fig. 2). At that time, the southern ice cap sublimes and releases large amounts of water vapor to the polar atmosphere. This water vapor is not easily transported toward the equator because the south polar region is isolated by a midlatitude westward summer vortex (*26*, *27*), except near eastern Hellas. There, the deep Hellas Basin forces a stationary planetary wave that results in a strong northward flow that transports large amounts of water out of the polar region (fig. S2). The moist and warm polar air meets colder air coming from northern Hellas, and the subsequent cooling results in strong condensation and precipitation (Fig. 4 and fig. S3). This is a robust mechanism that should not be model-dependent (*28*).

For all the simulations presented here, some quantitative uncertainties remain, because our model is designed to simulate present-day Mars and does not include some processes that may be substantial at high obliquity, like the radiative feedback of water vapor and ice clouds or the scavenging of dust out of the atmosphere. The amount of dust lifted into the atmosphere may also have been different (*28*, *29*). Additional simulations suggest that more atmospheric dust means less ice condensation because dust tends to warm the atmosphere.

The formation of glaciers on Mars appears to be the product of the same martian climate system as that of today, except that high obliquity increases the atmospheric water content and amplifies the circulation. In reality, the complex variations of orbital parameters probably led to several different types of regimes in the past, with water ice alternatively mobilized from the poles to tropical and midlatitude glaciers and then back to high latitudes to possibly form the meters-thick deposits whose remnants have been detected by the Mars Odyssey Gamma Ray Spectrometer (*16*). We do not predict glacier formation in the Deuteronilus–Protonilus Mensae area and other similar areas in the northern midlatitudes. These accumulations might have involved climate changes due to other origins (impacts, volcanism, or catastrophic outflows). However, some combination of orbital parameters or a higher model resolution may be sufficient to simulate ice precipitation in this region without invoking other processes. The mobilization of ice to the low and midlatitudes in preferred locations such as Eastern Hellas also supports a simple, purely atmospheric scenario for the origin of many of the martian gullies (*29*).

References and Notes

1. J. W. Head *et al.*, *Nature* **434**, 346 (2005).
2. G. Neukum *et al.*, *Nature* **432**, 971 (2004).
3. J. W. Head, D. R. Marchant, *Geology* **31**, 641 (2003).
4. D. E. Shean, J. W. Head, D. R. Marchant, *J. Geophys. Res.* **110**, E05001 (2005).
5. T. L. Pierce, D. A. Crown, *Icarus* **163**, 46 (2003).
6. W. K. Hartmann, T. Thorsteinsson, F. Sigurdsson, *Icarus* **162**, 259 (2003).
7. E. Hauber *et al.*, *Nature* **434**, 356 (2005).
8. S. M. Milkovich, J. W. Head, D. R. Marchant, *Icarus*, in press.
9. S. W. Squyres, *J. Geophys. Res.* **84**, 8087 (1979).
10. B. K. Lucchitta, *Icarus* **45**, 264 (1981).
11. P. R. Christensen, *Nature* **422**, 45 (2003).
12. B. K. Lucchitta, *J. Geophys. Res.* **89** (suppl.), 409 (1984).
13. N. Mangold, *J. Geophys. Res.* **108,** 10.1029/2002JE001885 (2003).
14. B. M. Jakosky, M. H. Carr, *Nature* **315**, 559 (1985).
15. M. A. Mischna, M. I. Richardson, R. J. Wilson, D. J. McCleese, *J. Geophys. Res.* **108**, 16-1 (2003).
16. B. Levrard, F. Forget, F. Montmessin, J. Laskar, *Nature* **431**, 1072 (2004).
17. F. Forget *et al.*, *J. Geophys. Res.* **104**, 24155 (1999).
18. F. Montmessin, F. Forget, P. Rannou, M. Cabane, R. M. Haberle, *J. Geophys. Res.* **109**, E10004 (2004).
19. The visible dust optical depth is a measure of the amount of dust in the atmosphere. It is defined as the logarithm of the vertical extinction of radiation.
20. J. Laskar *et al.*, *Icarus* **170**, 343 (2004).
21. In practice, because such a model is too computationally expensive to be run for more than 2 years, we initialized the high-resolution simulation with the atmospheric water vapor predicted at the end of a 10-year identical run but performed the simulation with a lower resolution (3.75° by 5.625°). We then ran the model for 2 additional years at high resolution, at which point the atmosphere had come to an interannually repeatable state.
22. M. I. Richardson, R. J. Wilson, *J. Geophys. Res.* **107**, 7-1 (2002).
23. R. T. Clancy, M. J. Wolff, P. R. Christensen, *J. Geophys. Res.* **108**, 2-1 (2003).
24. P. Thomas, S. Squyres, K. Herkenhoff, A. Howard, B. Murray, in *Mars*, H. H. Kieffer *et al.*, Eds. (Univ. of Arizona Press, Tucson, 1992), pp. 767–795.
25. F. Montmessin, R. M. Haberle, F. Forget, *Proc. Lunar Planet. Sci. Conf.* **35**, 1312 (2004).
26. R. M. Haberle, J. R. Murphy, J. Schaeffer, *Icarus* **161**, 66 (2003).
27. C. E. Newman, S. R. Lewis, P. L. Read, *Icarus* **174**, 135 (2005).
28. Additional simulations performed with more atmospheric water provided to the system by assuming a south water ice cap enlarged by 5° latitude or by using present-day orbit (and thus a warmer southern summer) result in stronger deposition and ice deposits further east.
29. F. Costard, F. Forget, N. Mangold, J. P. Peulvast, *Science* **295**, 110 (2002); published online 29 November 2001 (10.1126/science.1066698).
30. D. H. Scott, K. L. Tanaka, *U. S. Geol. Surv. Misc. Invest. Map I-1802-A* (1986).

31. The LMD Martian global climate model has been developed with the support of CNRS, European Space Agency (ESA), and CNES in collaboration with the Atmospheric, Oceanic, and Planetary Physics group in Oxford University (UK). Much of this work was performed while F.F. was visiting the Space Science Division of NASA Ames Research Center as a Senior National Research Council fellow. We wish to thank J. Hollingsworth, J. Schaeffer, T. Colaprete, and C. P. McKay for their support and advice. The research was also strongly motivated by the recent results from the ESA Mars Express mission within the scope of the Interdisciplinary Scientist Program. J.W.H. thanks the NASA Mars Data Analysis Program for partial support.

Supporting Online Material

www.sciencemag.org/cgi/content/full/311/5759/368/DC1
Figs. S1 to S3

19 September 2005; accepted 15 December 2005
10.1126/science.1120335

South-Seeking Magnetotactic Bacteria in the Northern Hemisphere

Sheri L. Simmons,[1,2] Dennis A. Bazylinski,[3] Katrina J. Edwards[2]*

Magnetotactic bacteria contain membrane-bound intracellular iron crystals (magnetosomes) and respond to magnetic fields. Polar magnetotactic bacteria in vertical chemical gradients are thought to respond to high oxygen levels by swimming downward into areas with low or no oxygen (toward geomagnetic north in the Northern Hemisphere and geomagnetic south in the Southern Hemisphere). We identified populations of polar magnetotactic bacteria in the Northern Hemisphere that respond to high oxygen levels by swimming toward geomagnetic south, the opposite of all previously reported magnetotactic behavior. The percentage of magnetotactic bacteria with south polarity in the environment is positively correlated with higher redox potential. The coexistence of magnetotactic bacteria with opposing polarities in the same redox environment conflicts with current models of the adaptive value of magnetotaxis.

Magnetotactic bacteria form intracellular single-domain ferrimagnetic iron oxide (magnetite, Fe_3O_4) or iron sulfide (greigite, Fe_3S_4) crystals. The torque produced by these chains causes the cells to align and to swim with respect to local or induced magnetic fields (*1–3*). Magnetotactic bacteria are globally distributed at and below the oxic-anoxic interface in chemically stratified freshwater (*4–6*) and marine environments (*7–10*), where they can